Hydrodynamic Study in a Cone Bottom Stirred Tank Using Computational Fluid Dynamics

L. F. Cardona[1,2], J. E. Arismendy[1], G. C. Quintana[1] and H. H. Alzate[1†]

[1] *Pulp and Paper Research Group, Faculty of Chemical Engineering, Universidad Pontificia Bolivariana, Medellín 56006, Colombia*
[2] *Department of Basic Sciences, Universidad Católica Luis Amigó, Medellín 050034, Colombia*

†*Corresponding Author Email: hader.alzate@upb.edu.co*

ABSTRACT

Stirred tanks are often used in industrial applications to store and process liquids and solids. However, these systems have become an increasing challenge to improve and optimize these processes. Computational Fluids Dynamics (CFD) simulation predicts complex phenomena as hydrodynamics system performance. An optimal solution is found using an effective mesh scheme and selecting appropriate boundary conditions. This work aims to validate and describe the distribution velocities inside the tank using a rigorous turbulence model. Stirred tank with a diameter of 27 cm and an oval cone tip using a Rushton impeller (radial impeller) and a 4-blade impeller inclined at 45° (axial impeller) are performed. For both cases, hydrodynamics in the bottom tank is analyzed. In addition, the power and the pumping numbers for each impeller are studied. The overall results show that at the tip of the oval cone, the asymmetry in the mesh is improved, and the divergence in the solution is avoided. Also, the cone designer increased the turbulent kinetic energy, which can enhance the mixture process. A decrease in power impeller is shown when the axial type is applied at low Reynolds numbers; however, when the cone is introduced inside the tank and a radial impeller type is used, the impeller power values are increased. The overall results of CFD simulation are compared to experimental data and provide similar values with an absolute deviation below 4.46 %.

1. INTRODUCTION

The stirring process in single-phase and multiphase systems is applied in manufacturing processes, pharmaceutical, mineral processing, and biotechnology industries, among others (Xia & Sun, 2002; Coroneo et al., 2011). The above implies ensuring a better quality of products to provide thermal and mass uniformity in the tank (Pukkella et al., 2019). Other applications are based on the storage and processing of liquids and solids (Prabhu et al., 2021), easy collection of sediment at the bottom of brewing and winemaking production (Desobgo, 2018), water treatment (el Mezaini, 2006), storing chemicals that may settle or separate over time (Landucci et al., 2012), agriculture for storing and separating milk, collecting sludge from fish tanks, or processing manure (Couturier et al., 2009; Nagy & Juhasz, 2016), among others. These applications demonstrate that the stirring process, particularly in conical base tanks primarily used in different industries to settle or separate solids or liquids

mixtures. This operation's theoretical basis comes from the fundamental concept of fluid motion and heat and mass transfer interactions (McCabe et al., 2007; Mustafa et al., 2021). The aim of the stirred tank studies is the optimization of geometric and operation conditions. The type of impeller, number of baffles, the number of impellers, and type of tank belong to be parameters used by engineering designers (McCabe et al., 2007). In this order of ideas, the hydrodynamics inside the tank is an important topic for research.

Hydrodynamics is used in industrial applications to design stirred tanks and provide operation conditions and geometrical dimensions (Qi et al., 2013). Stirred tank design is still subject to approximations and uncertainties. Also, the non-appropriate design can produce billions of dollars in yearly losses (Montante et al., 2001). The hydrodynamic analysis behavior of complex systems including turbulent and multiphase flows (as is the case of stirred systems) implies the use of a Computational Fluid Dynamics (CFD) simulation which allows expressing the

NOMENCLATURE

$C_{\varepsilon 1}$	RNG (k-ε) model constant	Re	Reynolds number
$C_{\varepsilon 2}$	RNG (k-ε) model constant	SM	Sliding Mesh
$C_{\varepsilon 3}$	RNG (k-ε) model constant	t	time (seconds)
C_{ε}	RNG (k-ε) model constant	T	tank diameter
D	impeller diameter	T_{emp}	temperature
D_{ij}	turbulent diffusion	$u_{i,j,k}$	velocity of fluid
FM	frame Motion	$u'_{i,j,k}$	velocity fluctuation component
g_i	gravity	α_k	RNG (k-ε) model constant
G_{ij}	production of pushing	β	RNG (k-ε) model constant
LES	large eddy simulation	ε_{ij}	dissipation term
N	rotation speed	ε	viscous dissipation rate
N_Q	pumping Number	θ	RNG (k-ε) model constant
N_P	Power Number	μ	dynamic viscosity
M	Match Number	μt	turbulent viscosity
P_{ij}	stress production	ρ	fluid density
QUICK	Quadratic Upstream Interpolation for Convective Kinematics	Φ_{ij}	pressure term
RANS	Reynolds-averaged Navier–Stokes equations	T	torque
P	power		

three circulating flow dimensions (radial, tangential, and axial) at the turbulent flow on all geometrics regions of the tank (Guha et al., 2008). CFD simulation provides information about the flow fields where considerable turbulence and energy losses are inside the tank. Also, these simulations are based on real process dimensions avoiding uncertainties generated in scaling (Micale et al., 2000). The energy costs of engine power used to the impeller drive at the stirred speed in a single phase are related to liquid volume, tank geometry, size and shape of the impeller, and fluid properties (Doran, 1995; Chapple et al., 2002). It is important to note that CFD simulation is successfully applied in applications such as compressor impellers (Nili-Ahmadabadi et al., 2014), ventilation rates in a cross Ventilated Rooms (Sivakumar et al., 2017), the aerodynamics of a wind turbine (Tahani & Moradi, 2016), among others.

Chudacek (1985) proposed a geometric alternative to decrease energy consumption in stirred systems with suspended solids. This author modified the bottom of the tank with a "cone and fillet." Also, the power consumption is improved to determine the minimum rotation speed of the impeller with the lower power consumption. This author shows the profiled tank is more efficient for off-bottom suspension and the use of cone and fillet tank geometry shows similar efficiency as the fully profiled bottom tank. Later, Wu & Patterson (1989) did experimental tests of a stirred system with a Rushton turbine with a volume of 15.45 L (liters) and a tank diameter of 27cm. These authors determined the radial velocity, the axial velocity, and the turbulent kinetic energy patterns at seven radial positions of the tank by Doppler techniques with a laser. These authors did an energetic analysis and found that 60% of the energy transmitted into the tank via the impeller was dissipated in that region and 40 % in the bulk of the tank. Zadghaffari et al. (2009) have done a simulation and validation study using several variables such as the flow field, power, and mixing time in a fully baffled stirred vessel with two six-blade Rushton turbines. CFD, sliding mesh (SM)

approaches and the large eddy simulation (LES) as the turbulence model are used. Also, three different impeller rotational speeds are applied: 225, 300, and 400 rpm. The overall results show that the normalized pumping flow rate is independent of the impeller speed and the impeller speed of 400 rpm shows different behavior compared to the other speeds. Finally, the experimental and simulated comparison is made, and the results show deviations below 4 %.

Youcef et al. (2016) performed an experimental and design study based on a tank with baffles. The results show an improvement in the radial speed in the mixing processes and no significant changes in power consumption. Also, the Rushton impeller is modified to estimate the energy consumption in the mixing process. These authors found an energy saving of around 18 % compared to the original impeller. Finally, concluded that CFD simulation is an appropriate tool for describing stirred tank systems. Later, these results were verified in Su et al. (2018) work.

Robust models should be included in the simulation to provide stirred tank designs closer to experimental behavior. k-epsilon (k-ε) or Reynolds-averaged Navier–Stokes equations (RANS) models belong to this category. The turbulence model becomes a significant challenge in CFD modeling (Mendoza-Escamilla et al., 2018). Mendoza-Escamilla et al. (2018) estimated the velocity fields and the torque at a rotation speed of 500 rpm in a stirred system with a 4-blade impeller inclined. These authors have done a CFD modeling using the κ-ε turbulence model with dense meshes and high influence on the walls where the pumping and power numbers approximate the experimental data.

Coroneo et al. (2011) studied RANS (Reynolds-averaged Navier–Stokes equations) simulation in stirred systems using CFD simulation and different turbulence models. These authors compared them to experimental data provided by Wu & Patterson (1989). These authors have done size and mesh changes using first and second

orders and QUICK (Quadratic Upstream Interpolation for Convective Kinematics) in the discretization schemes for solution methods of partial differential equations with frame motion. The results indicate inherent limitations in the turbulence model associated with RANS simulations that cannot describe the fluid mixtures in stirred tanks, especially dissipation and anisotropy turbulence energies. Singh et al. (2011) studied different turbulence models. The authors found that the κ-ε model poorly predicts turbulent energy dissipation at boundary positions of the impeller and the SSG-RSM turbulence model (SSG: Speziale-Sarkar-Gatski, and RSM: Reynolds Stress Models) provides adequate results, however, requires a high computational effort. To improve this limitation different researchers studied stirred tanks simulation and the RANS turbulence model that obtained appropriate results (Van den Akker, 2006). Delgadillo & Rajamani (2005) made an experimental and simulation comparison of turbulence for hydrocyclones. The results indicate that the LES (Large Eddy Simulation) provides low deviation compared to the RANS model.

Devi & Kumar (2011, 2012) performed a simulation with a CD-6 type impeller, a κ-ε turbulence model, and stationary reference fields. The main conclusion is that the CD-6 impeller shows a better mix than the Rushton-type impeller (Wu & Patterson, 1989) because it presents better turbulent kinetic energy in the points adjacent to the impeller. Also, energy-saving strategies show lower power consumption than the Rushton impeller. Another interesting study performed with the CD-6 type impeller (radial flow), is the one performed by Khapre & Munshi (2014). These authors demonstrate that the magnitude of the velocity produced by the CD-6 type impeller is smaller than that of the Rushton type impeller, however, the radial velocity near the impeller blade is higher than that of the Rushton impeller. Also, the Power and pumping numbers generate appropriate results compared to experimental values (Wu & Patterson, 1989). Liangchao et al. (2019) performed a CFD study in a Rushton turbine-stirred tank. The operating condition, working medium and geometrical parameter, flow field, and power numbers are evaluated. The main results found in this study are that the velocity at impeller height decreases for thicker blades and the Reynolds number knowledge provides information about all the variables studied. For example, the power number falls when increased of Reynolds number and this number is similar when the tank is an unbaffled and baffled tank. Naeeni & Pakzad (2019) studied the droplet size distribution and the mixing hydrodynamics in a stirred tank with a Rushton turbine. CFD simulation coupled with population balance modeling (PBM) is applied in a water and crude oil mixture. Also, the Eulerian multiphase model and standard k-ε turbulence model are used to describe the flow field. These authors found that the higher impeller speed provides predominant breakage in the system and smaller droplet changes. A current study of a stirred tank (Baba et al., 2022) identifies the dead flow zone at the bottom of the tank. The results of this work indicated that 5 blades impeller provides a broader region of high-velocity magnitude distribution and a higher distribution of velocity magnitude. Also, the number of blades is insignificant in the region close to the rotating

(a)
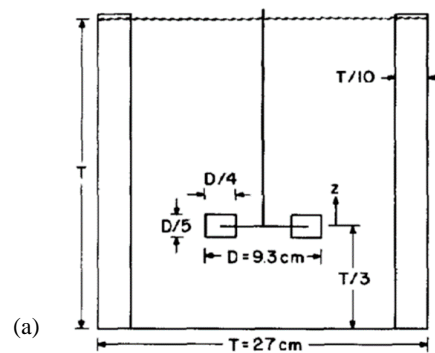
a) Dimensions of the stirred tank analyzed (Devi & Kumar, 2012)

(b)   (c)
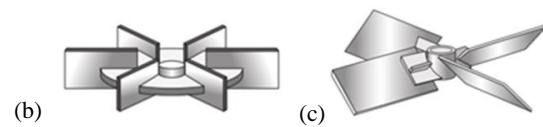
b) Rushton impeller and c) 4-blade impeller 45° inclined (Pitched-blade turbine)

Fig. 1 Characteristics of the stirred tank

impeller.

This work aims to provide hydrodynamic behavior information on the stirred tank system employing two different types of impellers and incorporating turbulent modeling. The Rushton and four-bladed pitch turbine with an angle of 45° (commonly known as a Pitched-blade turbine) are simulated using different rotation speeds. The pattern of the different velocity components is evaluated using the CFD simulation tool. The CFD simulation results of stirred tanks are compared with the experimental study provided by Chudacek (1985). The main application of this study can be used to improve stirred tank conditions with two types of impellers evaluated or design new industrial processes.

2. METHODOLOGY

2.1 Stirred Tank Design.

In this work, the dimensions of the tank are the same applied by Wu & Patterson (1989). These authors did an experimental study in a cylindrical stirred system with four baffles with a diameter (T) of 27 cm, and a Rushton-type impeller (d) with a diameter of 9.3 cm. Pure water is used at standard conditions ($T_{emp} = 25$ °C, $P = 101.325$ kPa, $\rho = 10^3$ kg/m^3, $\mu = 10^{-3}$ Pa·s) with a rotation impeller speed is around 200 rpm (Zadghaffari et al., 2009). Figure 1 shows the dimensions of the stirred tank. Also, the Rushton impeller and 4-blade impeller 45° inclined are shown. With the above conditions, CFD simulation is applied in this research due to being a useful and dynamic software. To validate the simulation results, the authors compared experimental values (Wu & Patterson, 1989) to evaluate the accuracy and robustness of the simulation. According to the validation results, two additional analyses are done related to (i) Modifying the mixing tank

Grid of the agitated system
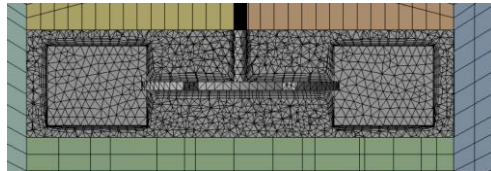
'Inner Region' of the Rushton impeller

Fig. 2 Grid and Inner characteristics of the stirred tank evaluated

Table 1 Grid none structured

Grid number 1		Grid number 12	
Tetrahedral Patch Independent		Tetrahedral Patch Independent	
# Elements	1963357	# Elements	1476439
# Nodes	371612	# Nodes	288370
Grid Quality		Grid Quality	
Skewness	0,627	Skewness	0.627
Aspect ratio	5.127	Aspect ratio	5.196
Orthogonality	0.43	Orthogonality	0.416
Quality of element	0.4065	Quality of element	0.400

geometry and (ii) Evaluation of the changed impeller by an axial type of 4 inclined blades of 45 ° (degrees). In both cases, qualitative and quantitative analysis behavior of the rotation speed is analyzed. Also, the power number curve (N_p) and the pumping number (N_Q) are done to compare the power consumption and the pumping capacity of the impeller ($Q=v_b \cdot A$ where $A=\pi \cdot (T/2)^2$ and v_b is the bulk velocity).

2.2 Grid Generation for Fluid Mechanics Computations

CFD simulation requires an appropriate meshing to find the solution to improve the computing time and prevent numerical divergence. Two unstructured meshes with an independent patch system are needed for problem-solving effects for stirred tanks. This system is solved by specifying two different sizes and three structured meshes with inflation in the impeller area due to the geometry complexity. Figure 2 shows the stirred tank's grid and inner region evaluated. Table 1 shows the values of unstructured mesh quality, while Table 2 shows the values selected for structured meshes with inflation in the impeller zone. On the other hand, CFD involves systems

analysis in fluid mechanics, heat transfer, and mass transfer, among others (Versteeg & Malalasekera, 2007). Particularly, the use of these simulations in fluid theory is a current topic applied in academia and industry to design and optimize different types of processes (Jakobsen, 2008).

2.2.1. Governing Equations

The numerical solution is based on the design of a mathematical model which includes ordinary, partial, and integral differential equations, which depend on boundary conditions and transport phenomena equations. Also, the coordinate system must be specified, and the numerical mesh required to solve the physical system. The numerical mesh generation requires a complete discrete representation of the geometric domains, and their solution is divided into finite numbers domain and sub-domains called elements or volumes. This mesh can be structured or unstructured (Versteeg & Malalasekera, 2007; Jakobsen, 2008). The discretized equations used in CFD simulation are solved in a 'Computer network'. In this work, the partial differential equations of the continuity equation and the Navier-Stokes equation are applied, and the mathematical representation is shown in Eqs. (1) and (2)

$$\frac{\partial \rho}{\partial t} + \rho \frac{\partial \langle u_i \rangle}{\partial x_i} = 0 \qquad (1)$$

Table 2 Grid Structured

Grid number 3		Grid number 4		Grid number 5	
Hexahedral on the tank, Tetrahedral + inflation on the impeller		Hexahedral on the tank + Tetrahedral on the impeller		Hexahedral on the tank + Tetrahedral on the impeller	
# Elements	380134	# Elements	227737	# Elements	267847
# Nodes	239457	# Nodes	367478	# Nodes	480115
Quality of the grid		Quality of the grid		Quality of the grid	
Skewness	0.897	Skewness	0.834	Skewness	0.845
Aspect ratio	4.739	Aspect ratio	4.1504	Aspect ratio	3.633
Orthogonality	0.198	Orthogonality	0.240	Orthogonality	0.198
Quality of element	0.124	Quality of element	0.239	Quality of element	0.225

$$\frac{\partial(\rho\langle u_i\rangle)}{\partial t} + \frac{\partial(\rho\langle u_i\rangle\langle u_j\rangle)}{\partial x_j}$$
$$= -\frac{\partial\langle p\rangle}{\partial x_i}$$
$$+ \frac{\partial}{\partial x_j}\left(\mu\frac{\partial\langle u_i\rangle}{\partial x_j}\right) \tag{2}$$
$$+ \frac{\partial}{\partial x_j}\left(-\rho\langle u_i'u_j'\rangle\right)$$
$$+ \rho g_i$$

In Eqs. (1) and (2), the subscripts $i,j = 1,2,3$ represent the coordinate system's component, ρ is the density of the fluid, u_i is the velocity of the fluid, p is the pressure and μ is the viscosity. Also, the term -ρ<u$_i$'u$_j$'> defines the Reynolds tensor and represents turbulent fluctuations. For the Reynolds tensor, different models are used in the literature and are described as follows (Delgadillo & Rajamani, 2005).

2.2.2. Turbulent Models

The turbulence is based on fluctuations in the flow field, in time and space. A complex flow described in three dimensions is unstable and has many scales that can significantly affect the stream. The turbulence is produced when the inertial force in the fluid has become significant over viscous forces and presents higher values in the Reynolds number ($R_e = \rho \cdot D^2 \cdot N \cdot / \mu$ where D is the impeller diameter, and N is the impeller rotational speed). The κ-ε turbulence model is simultaneously used to solve the turbulent kinetic energy per unit of mass equations (κ) and the dissipation rate per unit of mass (ε). High Reynolds number and turbulent viscosity (that must be isotropic) are applied in this work (Ansys Fluent 12, 2009).

On the other hand, the Reynolds Stress Model (RSM) is the most elaborate turbulence model found in the literature. When the isotropic turbulent viscosity hypothesis is rejected, the RSM completes the system is used. The RANS equations through the solution of transport equations for the Reynolds stresses and the dissipation rate equation is solved. The above means that 2-D flows are necessary four equations and in 3-D flows must be resolved seven additional transport equations. As RSM quantifies the different effects related to the curvature of the flow lines, the turbulence, the rotation, and the abruptness of flow change more rigorously than the models of the two equations.

Nevertheless, the prediction capability of RSM is limited for different terms of the exact transport equations for the transport of the Reynolds stresses. Also, modeling the pressure and dissipation rate is difficult and sometimes compromises the accuracy of RSM. On the other hand, RSM can spend more iterations to solve κ-ε, due to the strong coupling between the stresses of Reynolds and the flow average. Therefore, RSM is applied when the interest is to model the flow in an anisotropic medium (Ansys Fluent 12, 2009).

Reynolds stress tensor is defined as -ρ<u$_i$'u$_j$'> and is shown as follows.

$$\frac{\partial\left(\rho\langle u_i'u_j'\rangle\right)}{\partial t} + \frac{\partial\left(\rho\mu_k\langle u_i\rangle\langle u_j\rangle\right)}{\partial x_k}$$
$$= D_{ij} + P_{ij} + G_{ij} \tag{3}$$
$$+ \Phi_{ij} + \varepsilon_{ij}$$

The left terms in Eq. (3), represent the local derivative time and convection terms. The right side is composed of the turbulent diffusion (D_{ij}) model, the stress production (P_{ij}), the production of pushing (G_{ij}), the pressure term (Φ_{ij}), and the dissipation term (ε_{ij}). The above mathematical representation is shown in Eqs (4) to (8).

$$D_{ij} = \frac{\partial}{\partial x_k}\left(\rho\mu_k\langle u_i\rangle'\langle u_j\rangle'\langle u_k\rangle'\right)$$
$$+ p\left(\delta_{kj}\langle u_i\rangle' \right. \tag{4}$$
$$\left. + \delta_{ik}\langle u_j\rangle'\right)$$

$$P_{ij} = -\rho\left(\langle u_i\rangle'\langle u_k\rangle'\frac{\partial\langle u_j\rangle'}{\partial x_k} \right.$$
$$\left. + \langle u_j\rangle'\langle u_k\rangle'\frac{\partial\langle u_i\rangle'}{\partial x_k}\right) \tag{5}$$

$$G_{ij} = -\rho\beta\left(g_i\langle u_j\rangle'\theta + g_j\langle u_i\rangle'\theta\right) \tag{6}$$

$$\Phi_{ij} = +p\left(\frac{\partial\langle u_i\rangle'}{\partial x_j} + \frac{\partial\langle u_j\rangle'}{\partial x_i}\right) \tag{7}$$

$$\varepsilon_{ij} = -2\mu\left(\frac{\partial\langle u_i\rangle'}{\partial x_k}\frac{\partial\langle u_j\rangle'}{\partial x_k}\right) \tag{8}$$

Also, the modeling applied in this work includes the turbulent energy kinetic (κ described in Eq. (9)) and the dissipation rate (ε described in Eq. (10)), and the mathematical expressions are presented as follows.

$$\frac{\partial(\rho k)}{\partial t} + \frac{\partial(\rho k\langle u_i\rangle)}{\partial x_i}$$
$$= \frac{\partial}{\partial x_j}\left[\left(\mu + \frac{\mu_t}{\sigma_t}\right)\frac{\partial k}{\partial x_j}\right] \tag{9}$$
$$+ \frac{1}{2}\left(P_{ij} + G_{ij}\right)$$
$$- \rho\varepsilon(1 + 2M_t^2)$$

$$\frac{\partial(\rho\varepsilon)}{\partial t} + \frac{\partial(\rho\varepsilon\langle u_i\rangle)}{\partial x_i}$$
$$= \frac{\partial}{\partial x_j}\left[\left(\mu + \frac{\mu_t}{\sigma_t}\right)\frac{\partial\varepsilon}{\partial x_j}\right]C_{\varepsilon_1} \tag{10}$$
$$+ \frac{1}{2}\left(P_{ij} + C_{\varepsilon_3}G_{ij}\right)\frac{\varepsilon}{k}$$
$$- C_{\varepsilon_2}\rho\frac{\varepsilon^2}{k}$$

In Eq. (9), M is the Mach number, σ_k, C_μ, $C_{\varepsilon 1}$, and $C_{\varepsilon 2}$ take a constant value of 0.82, 0.09, 1.44, 1.92, respectively and $C_{\varepsilon 3}$ is a function of the flow in the direction of the gravitational vector (Singh et al., 2011; Youcef et al., 2016) and μ_t is the turbulent viscosity and is estimated using the Eq. (11) described as follows.

$$\mu_t = \rho C_\mu\frac{\varepsilon^2}{k}$$

2.3. Model for The Rotational System.

3-D impeller simulation is done with two models, based on a Multiple Reference Model (MRM) and Sliding Mesh.

2.3.1. Multiple Reference Model (MRM)

The Multiple Reference Model (MRM) is a numerical approximation around mobile parts, in this case, the impeller. MRM solves a simulation of a moving reference frame in a steady state with a constant rotational speed (Martínez-Nelis, 2010).

2.3.2. Sliding Mesh

Sliding Mesh is a solution dependent on time where the adjacent mesh to the rotatory component moves, while the solution is solving. The above means that the motion of the impeller is modeled in a way more realistic as the near mesh keeps moving the impeller, giving more accurate results between the impeller and tank (Martínez-Nelis, 2010).

CFD simulation was made in a Workstation Intel Xeon X5650 2.67 GHz, with 12 processors in parallel and an academic license from Instituto Tecnológico Metropolitano (ITM) located in Medellín, Colombia. The equations have been solved numerically using ANSYS FLUENT 17.0®, with a finite volume method to get the solution.

The following suppositions are applied and are described as follows.

a. The diameter of the tank is equal to the height of the tank.

b. Two turbulence methods RSM and κ-ε RNG on the walls in the tank are applied to analyze which method is more accurate concerning experimental data.

c. Two different systems for the moving reference frame are applied.

d. SIMPLE algorithm (Semi-Implicit Method for Pressure-Linked Equations) is applied.

e. PRESTO algorithm was used which is an interpolation scheme of the pressure. Also, this algorithm is used in swirl flows.

f. Second-order upwind system is used for pressure, momentum, and turbulent kinetic energy.

g. Fluid flow is a multi-phase model (Volume of Fluid, VOF). The meshes, the tank level, and the mesh partitions for water and air are considered.

3. RESULTS AND DISCUSSIONS

In this work, CFD simulation is analyzed and validated numerically with the experimental data reported by Wu & Patterson (1989). These authors have done a study in a stirred tank with a Rushton impeller through Lasser
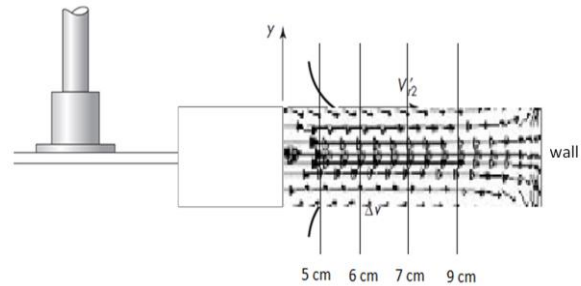
Fig. 3 Experimental measurements of radial velocity were performed for a Rushton-type

Doppler Velocity to measure the velocity magnitude and the radial velocity of six different positions from the impeller to the wall of the tank.

The mesh dependence is first analyzed using two turbulence models (κ-ε RNG and RSM) with three solution methods (First order upwind, second-order upwind, and QUICK). Also, two different moving reference frames (Frame Motion and Mesh Motion) are applied. However, the selection criteria for the mesh are related to the appropriate experimental data fit with the model and the mesh requiring less computational effort. Secondly, a different impeller with four inclined blades to 45 ° is included in the simulation results. The above implies doing a quantitative analysis of the pumping and power numbers. Thirdly, a cone on the bottom of the stirred tank is included in the simulation. The reason for doing this simulation is to describe the flow patterns in the tank and compare them with a flat base. The above is done using a Rushton and four inclined blade impellers.

3.1. Validation

Figure 3 shows the positions of the experimental measurements taken. As can be seen in this figure, different ratios from the Rushton-type impeller to the wall of the stirred tank are used. Also, in the validation procedure, the radial velocity of the impeller is compared due to the Rushton-type being a radial impeller. High computational efforts with Mesh 1 were obtained and had no solution after a week. Mesh 2 used an RSM turbulence model with mesh motion, the comparison of the results is shown in Fig. 4.

For a ratio of 5 cm, the maximum values of the radial velocities in the simulations do not provide appropriate results when compared to experimental data, i.e., mesh 2 is discarded for a dependence of mesh study.

The first analysis is done for a constant mesh 3, 4, and 5 for 2 different ratios of turbulence models (κ-ε RNG and RSM) coupled with three solution modeling related to the moving reference frame. The SIMPLE, Least-Squares Gradient, and PRESTO algorithms are also applied. The above is verified using first order upwind, QUICK for momentum phenomena, turbulent kinetic energy, and
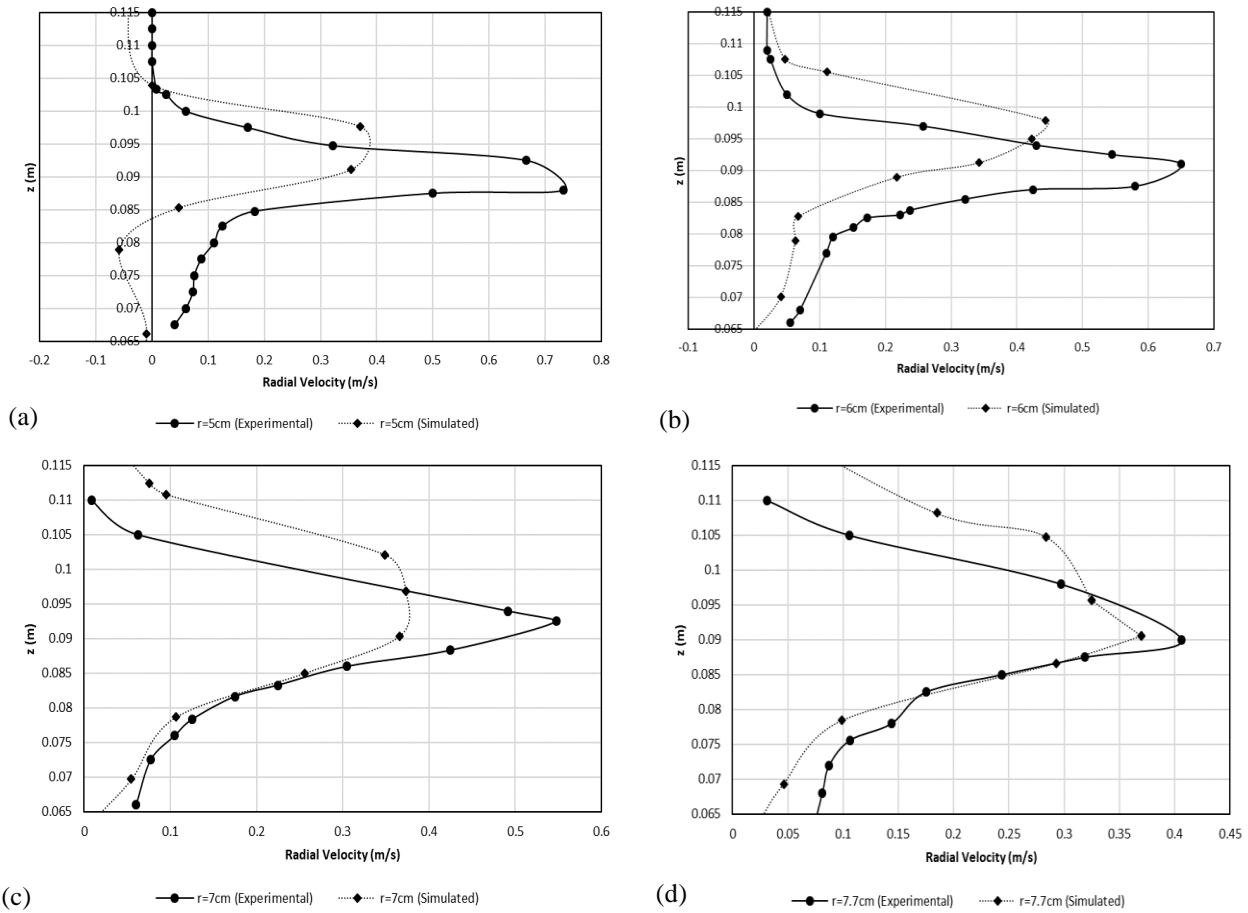
Fig. 4 Mesh 2 results for radial velocity in comparison with experimental data, a) r = 5 cm; b) r = 6 cm; c) r = 7 cm; r = 7.7 cm

dissipation algorithms. Figure 5 shows the overall results for mesh 5 at different ratios while Figs. 6 and 7 show the results for mesh 4 at 5 and 7 cm. Following these graphical behaviors, Fig. 8 shows the results for mesh 3 at 5 cm. In these figures, no changes in the solution are found. The simulation behavior of these figures is similar to those obtained from Wu & Patterson (1989). The turbulence model and the moving reference frame are defined. In the following analysis ratio of measurements remained constant and the variations in mesh for the RSM model and moving reference frame (Mesh Motion). The results previously obtained for the κ-ε model do not provide appropriate values as can be seen in Fig. 9. On the other hand, mesh 5 obtained satisfactory results with 267000 elements and 480000 nodes, and a skewness of 0.83. This simulation takes around three days to find a solution and the results can be seen in Fig. 10.

3.2. Pumping Number Validation

The pumping number (N_Q) is the capacity of the material discharged due to the rotation of the impeller. For this study, the pumping number is estimated by ANSYS for a radial impeller. To do this calculation the mass flow is modeled using a revolution surface around the impeller. Figure 11 shows the surfaces of revolution applied in this work (Bakker, 2006). As can be seen in this figure the

surface must be superimposed on the positions where the movement vectors of the impeller direct the fluid (guaranteed uniform flow). ANSYS results show that the motion vectors guided the fluid (Wu & Patterson, 1989) and show that the pumping capacity does not depend on the impeller velocity unto the wall of the stirred tank. Also, the validation indicates that a variation exists between the radial position and impeller velocity. The above is illustrated in Fig. 11. The experimental and simulation behavior is similar to other literature works (Wu & Patterson, 1989; Venneker et al., 2010) where the normalized pumping capacity is independent of the impeller speed and increases with radial distance from the impeller. The pumping capacity (Q/ND^3) at r/R = 1 is compared to Wu & Patterson (1989) compiled experimental data. These authors found Q/ND^3 for different turbine sizes spans between 0.73 and 0.89. Compared to our work, the Q/ND^3 varies in a narrow range between 0.73 to 0.79, i.e., the modeling results are within the experimental range reported in the literature.

**3.2.1. Validation of the Power Number**

For stirred tanks, knowing the power required to move the impeller is essential. Power number is a relationship between the types of fluid that the impeller uses and its

(a)

(b)

(c)
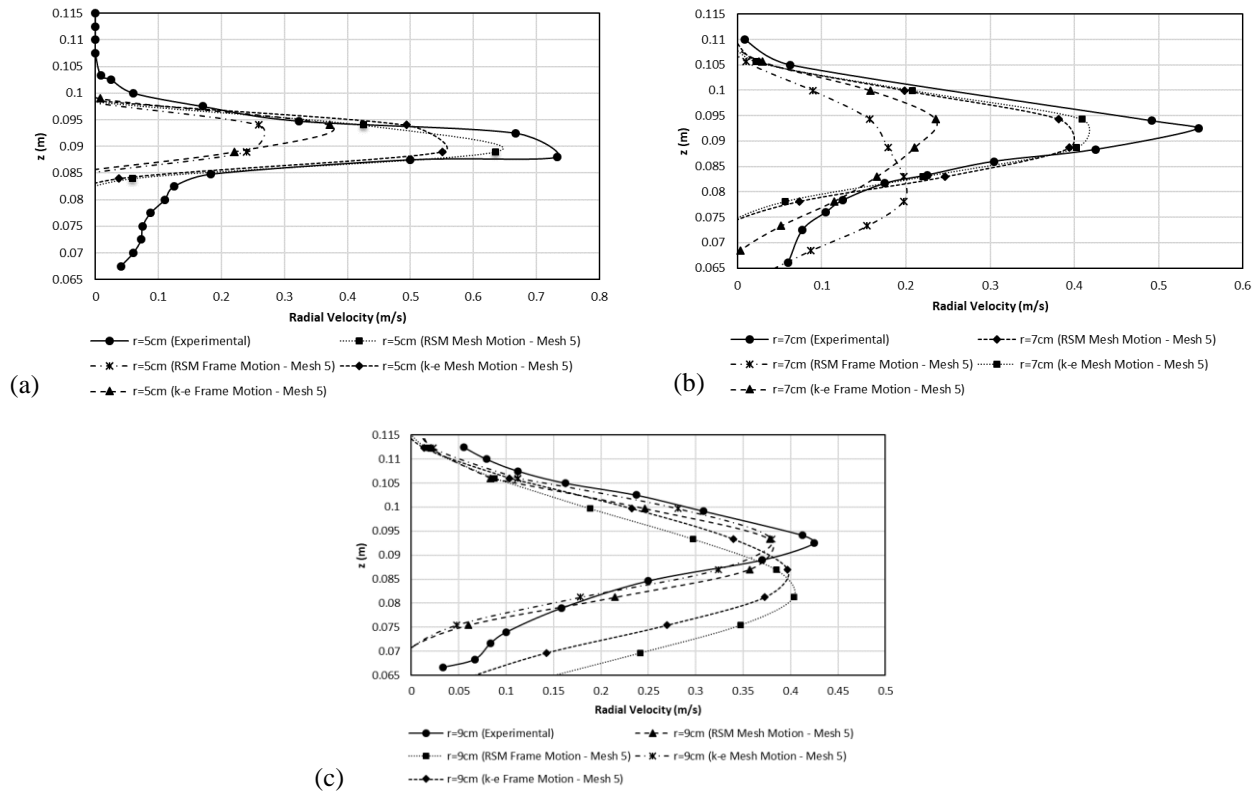
Fig. 5 Mesh 5 results with different measure ratios. a) radial position at 5 cm; b) radial position at 7 cm; c) radial position at 9 cm

(a)

(b)
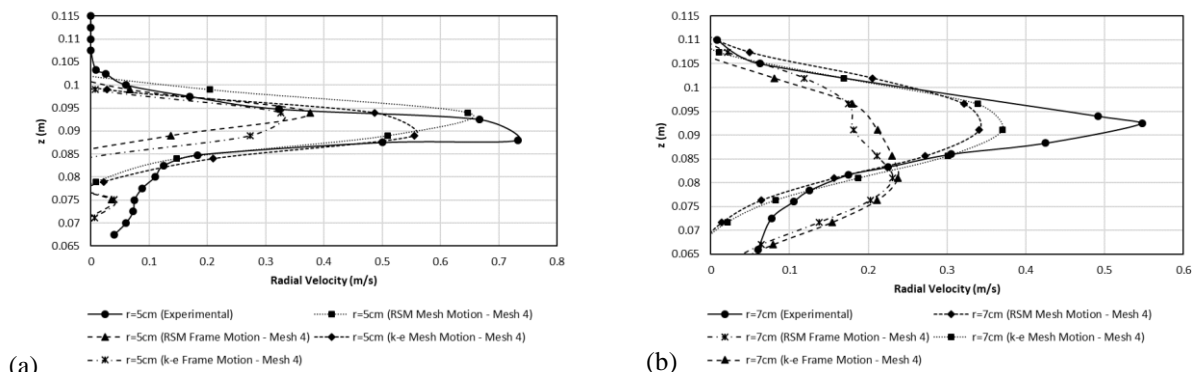
Fig. 6 Mesh 4 results with different measure ratios. a) radial position at 5 cm. b) radial position at 7 cm
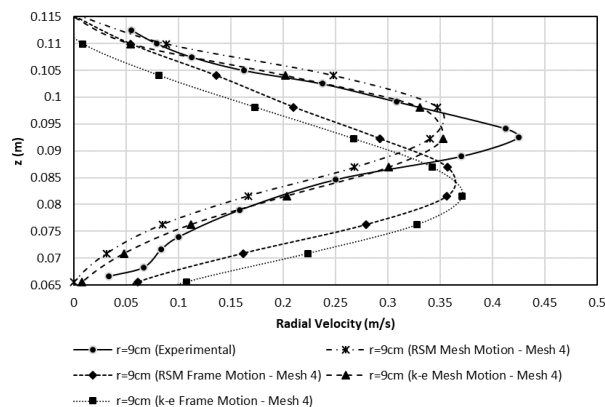
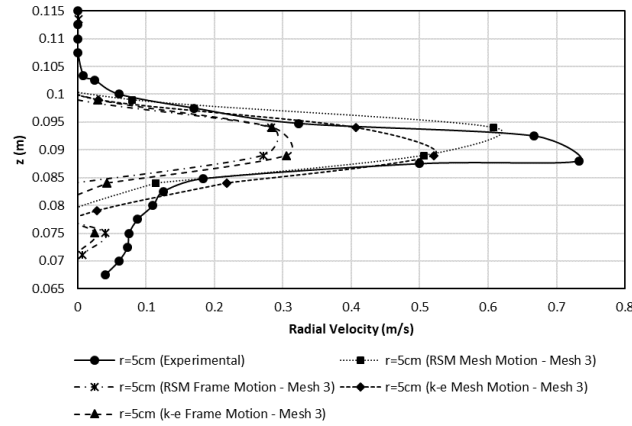**Fig. 7 Mesh 4 results with a radial position of 9 cm**
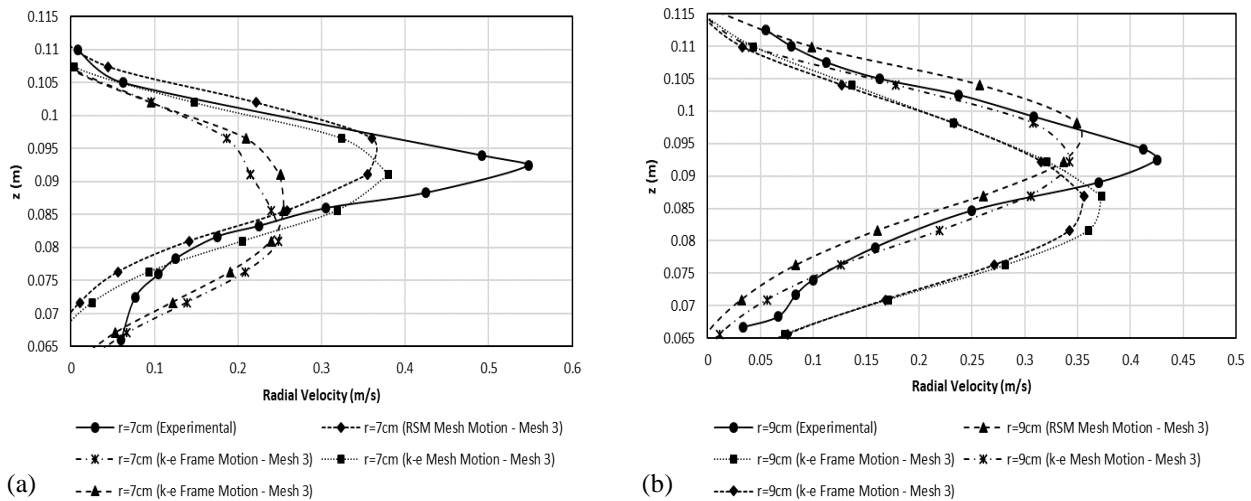
Fig. 8 Mesh 3 results with a radial position of 5 cm

Fig. 9 Mesh 4 results of different measure ratios. a) radial position at 7 cm. b) radial position at 9 cm

power. It depends on the diameter of the impeller, the type of impeller, the rotation speed if there are baffles, and the characteristics of the fluid. On the other hand, the power number is defined in Eq. (12) and can be seen as follows.

$$N_p = \frac{P}{\rho N^3 D^5} \qquad (12)$$

In Eq. (12), P is the impeller power (W), ρ is the fluid density (k/m³), N is the velocity of the impeller in (rps) and D is the diameter of the impeller (m). The ANSYS algorithm calculates the power number through the impeller shaft torque (T in N·m) described in Eq. (13) (Lane & Koh, 1997).

$$P = 2\pi N T \qquad (13)$$

Besides validating the flow patterns for a radial impeller, the pumping and power numbers are also validated. The power number for a Rushton impeller throw values of 4.67, and the value for each mesh is shown in Tables 3 and 4. The validation verified that mesh 5 provides adequate results compared to the experimental data with an average absolute deviation of around 0.17 %. For pumping numbers, the literature shows results of 0.73 for rotation speed between 100 to 350 rpm (Lane & Koh, 1997; Paul et al., 2004), and the simulation value of 0.75 reached an average absolute deviation of 2.74 %. This value indicates a good agreement of the simulation and the experimental data. As seen in these Tables the RSM FM and k-ε FM simulations provide absolute relative deviation (AD) of N_p and N_Q values above 24.87 % (the maximum deviation is around 38.96 %). This result indicates that these models using mesh 3 to 5 do not adequately describe the fluid flow pattern. Otherwise, RSM SM and k-ε SM present an absolute deviation below 11.68 % where the average absolute deviation is around 4.46 %, i.e., simulation reports are consistent with experimental data, so the authors recommended using these two models. It is important to clarify that the notation of RSM is related to the Reynolds Stress Models, SM is the Sliding Mesh and FM is the Frame Motion.
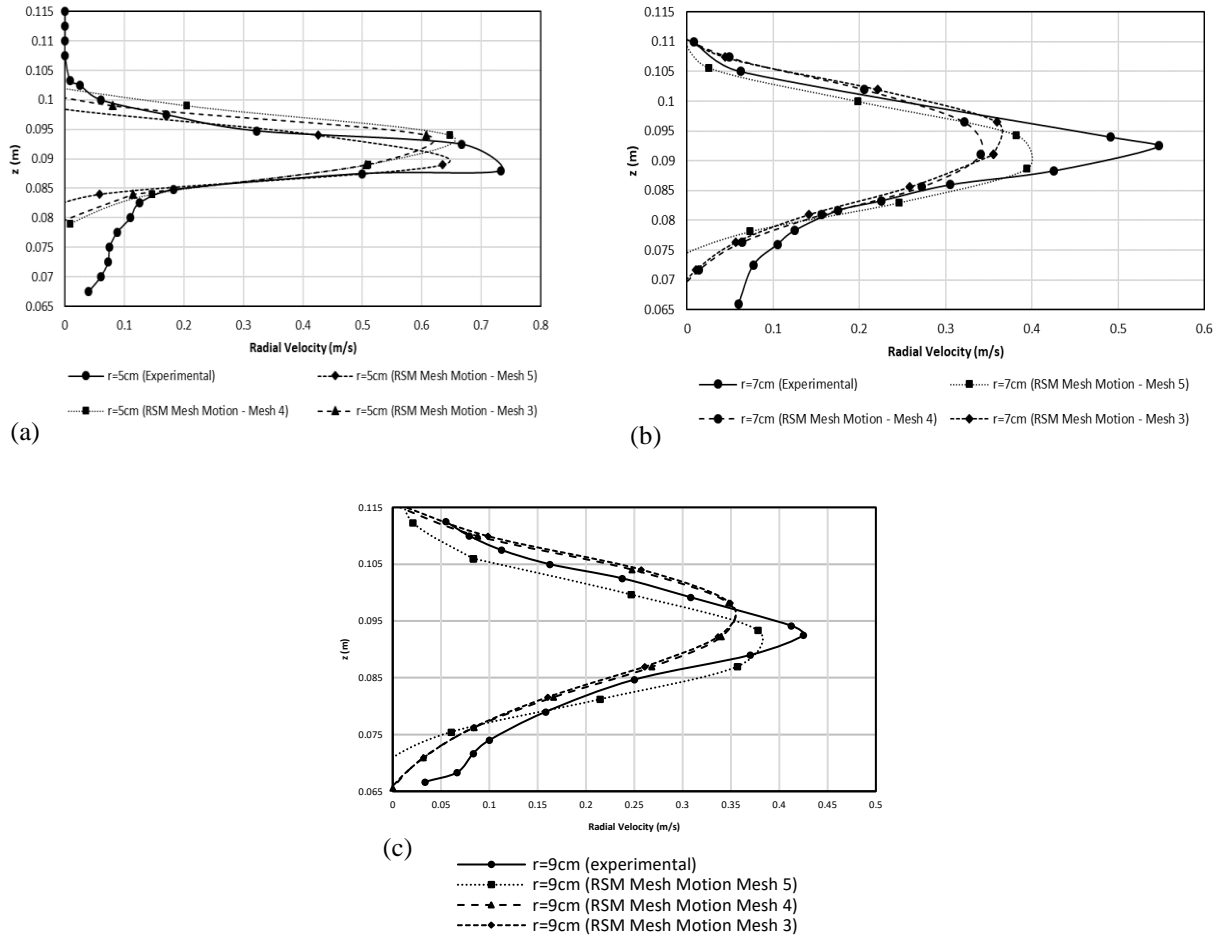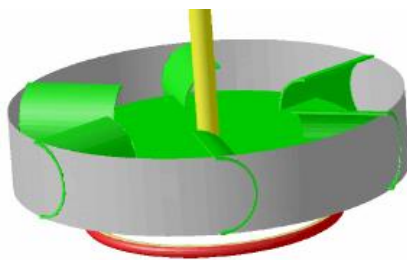
(a)

(b)

(c)

Fig. 10 Mesh variations results and the constant ratio
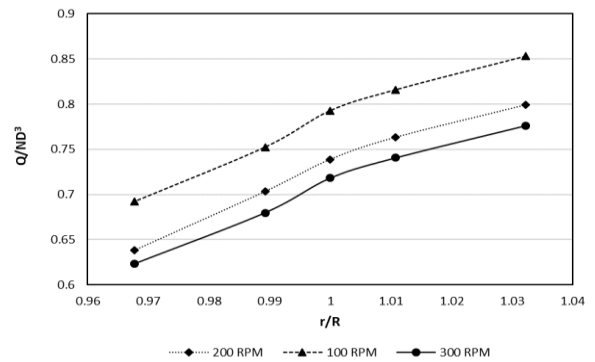

Revolution surface (Bakker, 2006)

Fig. 11 Pumping capacity

Table 3 Pumping and power numbers for mesh 3 and 4. AD is related to the absolute deviation

Models	Mesh 3				Mesh 4			
	N_Q	N_P	AD N_Q	AD N_P	N_Q	N_P	AD N_Q	AD N_P
RSM SM	0.69	4.56	5.42%	2.47%	0.66	4.59	11.03%	1.78%
k-ε SM	0.65	4.34	11.68%	7.65%	0.73	4.41	0.15%	5.79%
RSM FM	0.58	3.59	24.87%	30.12%	0.55	3.52	33.12%	32.61%
k-ε FM	0.58	3.47	25.83%	34.71%	0.54	3.48	34.40%	34.37%

Table 4 Pumping and power numbers for mesh 5

| Models	Mesh 5			
	N_Q	N_P	AD N_Q	AD N_P
RSM SM	0.75	4.68	2.86%	0.17%
k-□ SM	0.73	4.48	0.15%	4.35%
RSM FM	0.53	3.61	38.96%	29.28%
k-□ FM	0.54	3.59	36.14%	30.15%

3.3. Flow Patterns for a Rushton Impeller

The stirred systems with a Rushton impeller are modeled using CFD and similar results to experimental data are obtained. Figure 12 shows the flow direction through the tank, where the flow direction goes perpendicularly toward the impeller blades. Also, the most considerable amount of energy goes to the tank's wall, generating a flow division that goes up and down for the recycle flow again to the impeller. The above effect generates a dead zone in the center of the tank, i.e., causes energy that is not in use for the mixture. Dong et al. (2016) developed simulations comparing flat and circular tank bottoms, to improve recirculation in the corners. The results show that in a turbulent regime a dead zone is formed in the center due to the high recirculation and the generation of high tangential velocity, similar to those obtained in this work.

3.3.1. Flow Patterns for Four Inclined Blades 45 Degrees

The stirred tank system is simulated with a four-inclined blade to 45 degrees impeller and mesh 5 selected previously. Using the same boundary conditions and water at standard conditions (T_{emp} =25 °C, P = 101.325 kPa, ρ =10^3 kg/m^3, μ = 10^{-3} Pa·s (Zadghaffari et al., 2009)) with a rotation speed of the impeller was 200 rpm. Also, the RSM turbulence model and moving reference frame are used with the same geometry provided in Fig. 1. In this work, the flow behavior and the turbulent kinetic energy are analyzed as a qualitative study because there are no experimental data under the same conditions. However, pumping and power numbers can be validated.

Figure 13 shows the velocity behavior. As can be seen in this figure, the greatest energy can be found at the end of the bladed impeller due to the inclination that generates the flow going down toward the corners of the tank and the flow direction going back toward the top of the tank and return to the impeller by gravity.

Validation of the power and pumping numbers must be accomplished with the tank's specifications. One of these specifications is related to the diameter of the impeller, which must have 1/3 of the diameter of the tank and it must have 4 baffles (Versteeg & Malalasekera, 2007). According to the experimental values reported by Versteeg & Malalasekera (2007), the power number is around 1.27 and the pumping number is around 0.79. When is compared to the CFD simulation the power and


(a)

(b)
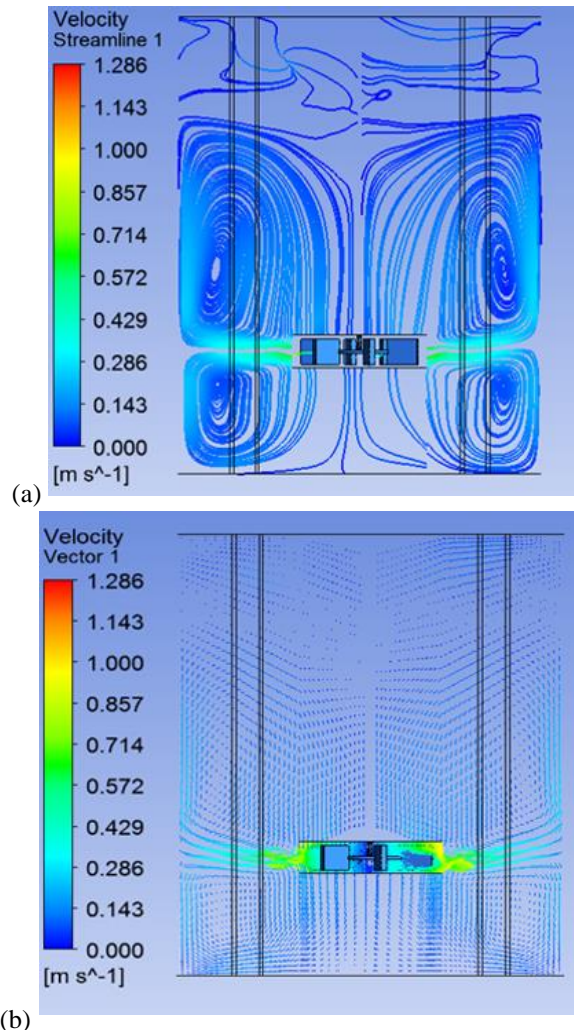
Fig. 12 Velocity magnitude of the Rushton impeller, a) Pathlines, b) Vectors

pumping numbers are around 1.32 and 0.82 and correspond to an absolute relative deviation of 4 %.

3.4. Geometric modifications at the Bottom of the Tank

Chudacek (1985) suggests a conic geometry in the center in order to improve the energy that cannot be used at the bottom of the tank. Following the recommendation of Chudacek (1985), an oval cone tip is applied to improve the skewness in the mesh and avoid divergence in the solution. Also, the ANSYS tool is used to make changes in the operational geometric variables. Figure 14 shows the geometric designer using Design Modeller ® software. This figure is done by modifying two types of impellers with the same operational conditions applied in the validation of the simulation.

When the CFD simulation is resolved a qualitative comparison between simulations at the bottom of the tank (with and without changes) and for each impeller is done. The variables related to the velocity vector, streamline, and turbulent kinetic energy is also used in the qualitative comparison. Figures 15 (velocity vectors), 16 (velocity streamline), and 17 (turbulent kinetic energy) illustrate the
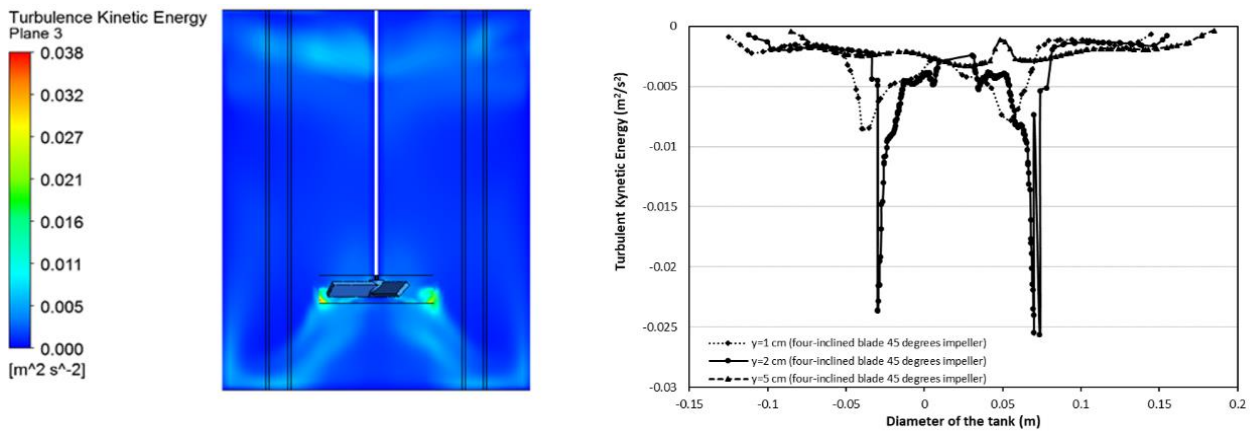
**Fig. 13 Turbulent kinetic energy for a four-inclined blade 45 degrees impeller**
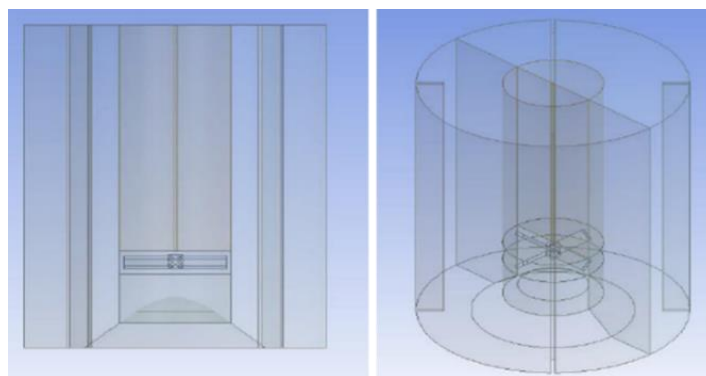
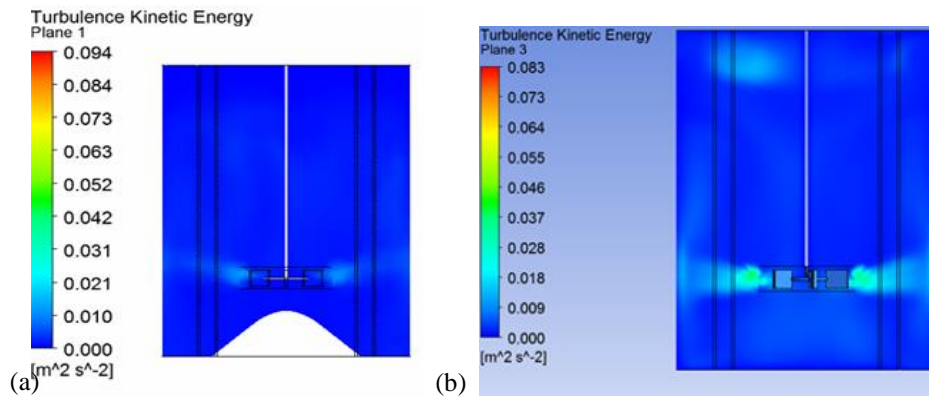**Fig. 14 Geometry of the tank with modifications in the bottom (right side)**
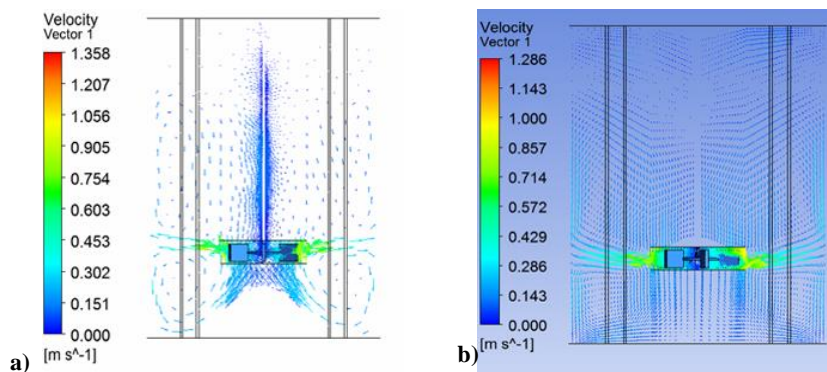
Fig. 15 Comparison of the flow patterns (velocity vectors) in a Rushton impeller a) with modifications and b) without modifications

contours of the Rushton impeller. As shown in Figs 15 to 17, the direction of the flow through the tank is perpendicular to the impeller blades, and they transmit their greatest energy to the tank walls. These generate a division up and down so that the flow is recirculated back to the impeller; this effect causes a dead zone to be generated in the center of the agitated system, in which energy is not being used at the time of mixing. The above can be corroborated when the turbulent kinetic energy in the stirred system is analyzed since the points where there

is no mixing, and this value is zero. The maximum turbulent kinetic energy of the fluid motion occurs in the impeller's discharge. As the fluid reaches the wall, it loses energy, and the recirculation movement towards the impeller is favored by the effect of gravity and drag in the tank. Also, Figs. 18 to 20 show the four blades inclined at 45° impeller. The stirring process for a four-blade inclined impeller at 45 ° impeller is simulated. Figures 18 and 20 show growing up turbulent kinetic energy. These figures show growing up turbulent kinetic energy at the tip of the
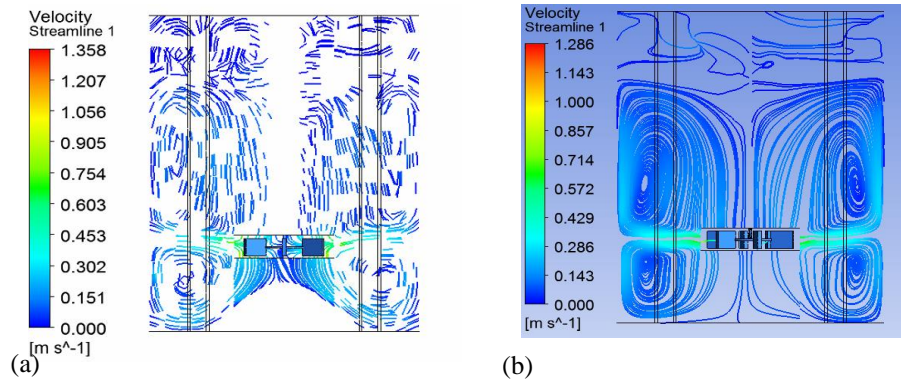
Fig. 16 Comparison of the flow patterns (velocity streamline) in a Rushton impeller a) with modifications and b) without modifications

Fig. 17 Comparison of the flow patterns (turbulent kinetic energy) in a Rushton impeller a) with modifications and b) without modifications
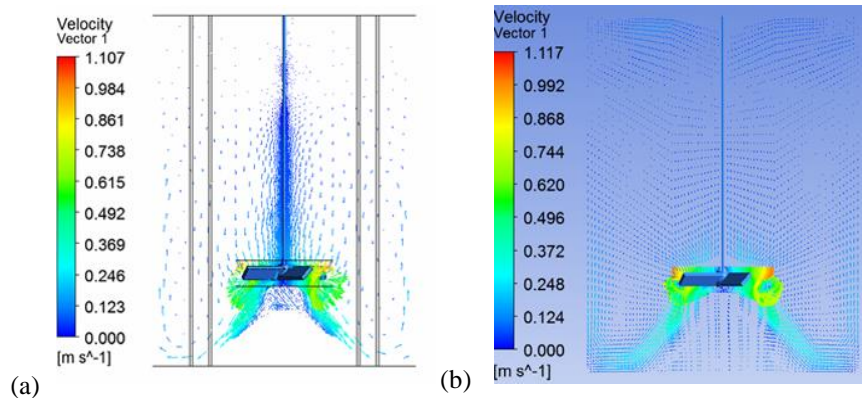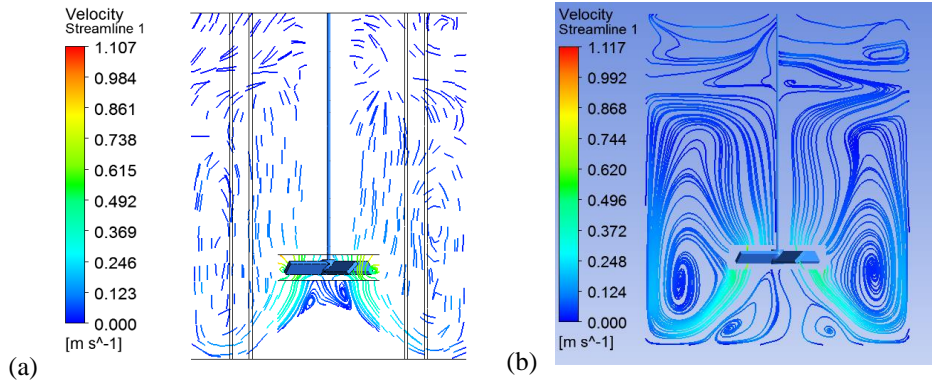

Fig. 18 Comparison of the flow patterns (velocity vectors) in a four-blade inclined impeller at 45 degrees a) with modifications and b) without modifications

impeller; however, it is inclined and directs the flow toward the corners of the tank, and also, the energy is directed back to the top. In the case where the geometry has been changed due to the less magnitude in the velocity vector at the bottom tank is accumulated at the tip of the cone generating an increase. As in the Rushton turbine, problems are also generated in the center of the tank, where is minimal effect of turbulent kinetic energy. Therefore, including the cone at the bottom of the tank improves the mixing or can avoid sedimentation in a suspension of solids. In this order of ideas, the energy in

the tank is maximized; however, the reduced tank's capacity is a limitation of the system.

3.5. Variation of the Rotation Speed in the Impeller

The variations of the rotational speed for each impeller and the geometrical modifications in the tank are analyzed. Also, the pumping and power numbers change are studied. For the four-blade inclined impeller, it is observed that for a low rotational speed the power number increase until a Reynolds number of 30000 after that it decreases to become constant. If the power number is

(a)

(b)

Fig. 19 Comparison of the flow patterns (velocity streamlines) in a four-blade inclined impeller at 45 degrees a) with modifications and b) without modifications
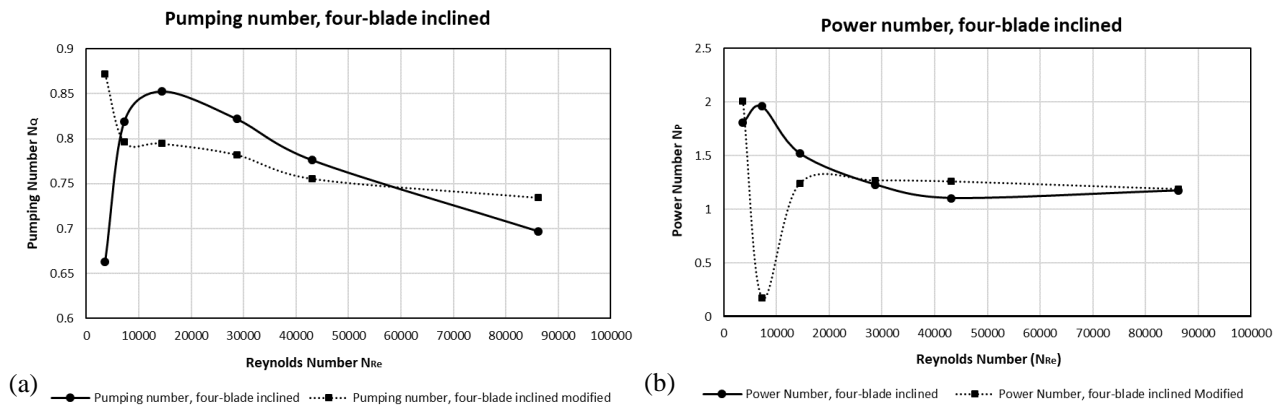

(a)

(b)
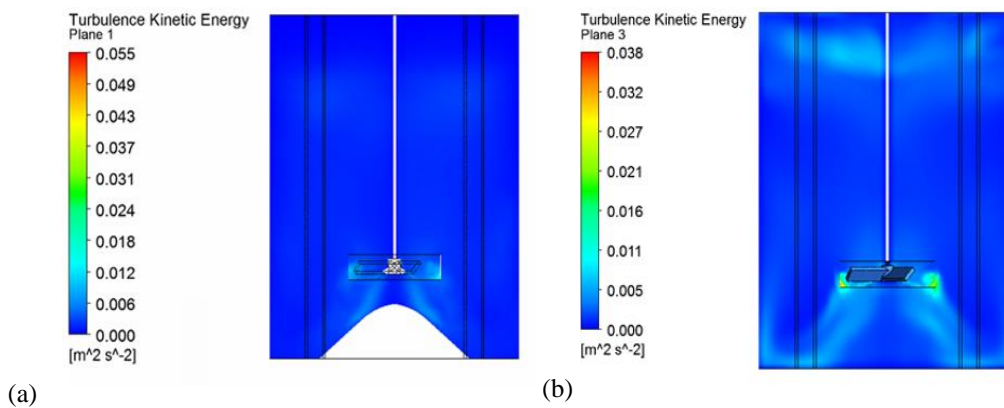
Fig. 20 Comparison of the flow patterns (turbulent kinetic energy) in a four-blade inclined impeller at 45 degrees a) with modifications and b) without modifications

(a)

(b)
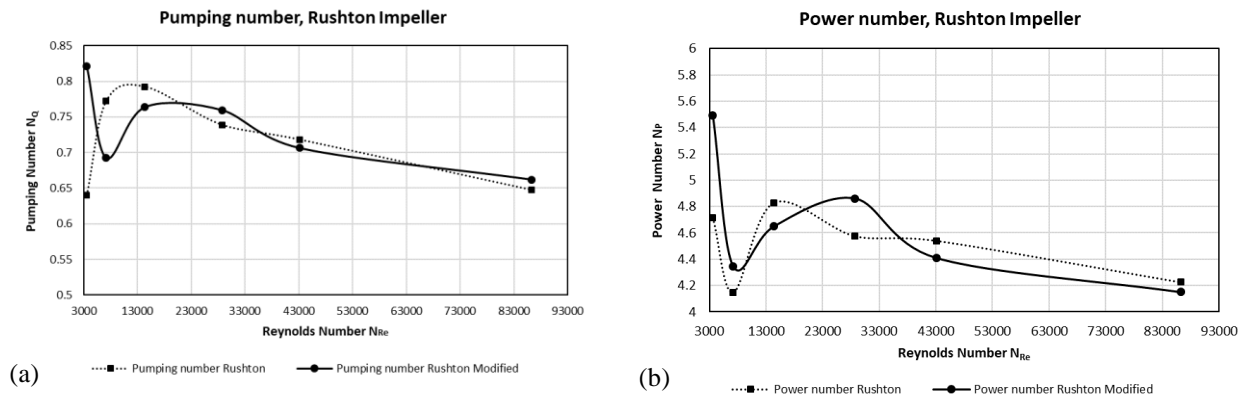
Fig. 21 Power Number in a Rushton impeller a) with modifications and b) without modifications

known is important to decide which rotation speed can generate without expending more energy (the optimal conditions of a mixing process). Figures 21 and 22 show the N_Q vs N_{Re} and N_P vs N_{Re} for both impellers under study. The bottom changes in the tank increased the internal flow with a lower energy consumption than the flat bottom tank system. This phenomenon occurs as well in the four-blade inclined impeller, however, less consumption of power in lower rotation speeds can be caused by the impeller type.

As can be seen in these figures, the power curves at different Rushton types do not collapse into one curve and provides different performances. For the power number (Fig. 21b) using a Rushton impeller presents at a low Reynolds number a concave upward change and with a high Reynolds number provides low numbers of values and reflects the local turbulence generation (Todaro & Vogel, 2014).

Pumping number, four-blade inclined

Power number, four-blade inclined

(a)

—●— Pumping number, four-blade inclined   ····■···· Pumping number, four-blade inclined modified

(b)

—●— Power Number, four-blade inclined   ····■···· Power Number, four-blade inclined Modified

Fig. 22 Power Number in a four-blade inclined impeller at 45 °. a) with modifications and b) without modifications

4. CONCLUSIONS

The following conclusions can be drawn and are described as follows.

In this work, an evaluation study is done in a stirred system to analyze the flow pattern under adequate boundary conditions. The CFD simulation is applied to model a stirred tank to describe the motion behavior of the flow during the mixing in a stirred tank. CFD designing uses a discretization searching for the adequate mesh to provide less computational effort and less response time

to obtain the desired solution. The RSM is selected with a moving reference frame (Mesh Motion) for the control volume around the impeller. According to the simulation values in the center of the stirred tank, there are velocity vectors that do not have an incidence which implies that are zones with an inefficient use of energy that is not being used properly.

The pumping capacity is done using different rotational speeds. The flow is directly proportional to the velocity, and it is linear when the ratio is increased. The power number is directly proportional to the power of the impeller and inversely to the rotational speed. Also, at low values of the power number and when the rotational speed increases the trend of this number decreases until it becomes constant. An advantage of the CFD tool is the facility to change geometrical conditions. In order to validate the simulation, a qualitative study of the dependence of mesh with an axial impeller is applied.

A cone on the bottom of the stirred tank is designed and compared with a flat bottom. The cone results provide an increase in the turbulent kinetic energy, and it can improve the mixture process, however, that sacrifices the capacity of the tank. On the other hand, this change on the bottom of the tank is useful for energy savings because when the tank has the cone in the bottom it produces more flow at less power and rotational speed. Similar simulation and experimental values are obtained with an overall absolute deviation below 4.46 %. This deviation value is

similar to those obtained in the literature (Zadghaffari et al., 2009). In this order of ideas, including the cone at the bottom of the tank improves the mixing and can avoid sedimentation in a suspension of solids. In this order of ideas, the energy in the tank is maximized; however, the reduced tank's capacity is a limitation of the system.

Further studies must be done using a Large Eddy Simulation model to improve the simulation results. This model is applied for detecting turbulent microscopic structures in transitory flows to describe a more accurate flow pattern. Also, another point to improve is the inclusion of some geometries in the corners on the bottom of the tank with the limitation of decreasing the capacity.

CONFLICT OF INTEREST

The authors declare that they have no known competing financial interests or personal relationships that could have appeared to influence the work reported in this paper.

AUTHORS CONTRIBUTION

Luis F. Cardona: Methodology, Validation, Writing – review & editing. **Juan E. Arismendy**: Methodology, Investigation, Software, Formal analysis, Writing – review & editing, Software. **Germán C. Quintana**: Conceptualization, Methodology, Investigation, Validation, Formal analysis, Writing – review & editing. **Hader H. Alzate**: Formal analysis, Conceptualization,

Methodology, Validation, Writing – review & editing, Software, Supervision, Project administration.

REFERENCES

Ansys Fluent 12. (2009). *Fluid Simulation Software*. (version 12) [software]. https://www.ansys.com/products/fluids/ansys-fluent

Baba, A. F., Samiran, N. A., Abd Rashid, R., Ishak, I. A., Salleh, Z. M., Madon, R. H., & Hamid, M. S. S. (2022). Effect of impeller's blade number on the performance of mixing flow in stirred tank using CFD simulation method. *CFD Letters*, 14(5), 33-42. https://doi.org/10.37934/cfdl.14.5.3342

Bakker, A. (2006). Modeling Flow Fields in Stirred Tanks: Reacting Flows - Lecture 7(FLUENT). https://www.bakker.org/

Chapple, D., Kresta, S. M., Wall, A., & Afacan, A. (2002). The effect of impeller and tank geometry on power number for a pitched blade turbine. *Chemical Engineering Research and Design*, 80(4), 364-372. https://doi.org/10.1205/026387602317446407

Chudacek, M. W. (1985). Solids suspension behaviour in profiled bottom and flat bottom mixing tanks. *Chemical Engineering Science*, 40(3), 385-392. https://doi.org/10.1016/0009-2509(85)85100-9

Coroneo, M., Montante, G., Paglianti, A., & Magelli, F. (2011). CFD prediction of fluid flow and mixing in stirred tanks: Numerical issues about the RANS simulations. *Computers & Chemical Engineering*, 35(10), 1959-1968. https://doi.org/10.1016/j.compchemeng.2010.12.007

Couturier, M., Trofimencoff, T., Buil, J. U., & Conroy, J. (2009). Solids removal at a recirculating salmon-smolt farm. *Aquacultural Engineering*, 41(2), 71-77. https://doi.org/10.1016/j.aquaeng.2009.05.001

Delgadillo, J. A., & Rajamani, R. K. (2005). A comparative study of three turbulence-closure models for the hydrocyclone problem. *International Journal of Mineral Processing*, 77(4), 217-230. https://doi.org/10.1016/j.minpro.2005.06.007

Desobgo, S. C. Z. (2018). Modernization of fermenters for large-scale production in the food and beverage industry. *Innovations in Technologies for Fermented Food and Beverage Industries*, 189-220. https://doi.org/10.1007/978-3-319-74820-7_11

Devi, T. T., & Kumar, B. (2011). Analyzing flow hydrodynamics in stirred tank with CD-6 and Rushton impeller. *International Review of Chemical Engineering*, 3(4), 440-448.

Devi, T. T., & Kumar, B. (2012). CFD simulation of flow patterns in unbaffled stirred tank with CD-6 impeller. *Chemical Industry and Chemical Engineering Quarterly*, 18(4-1), 535-546. https://doi.org/10.2298/CICEQ111130029D

Dong, J., Hu, B., Pacek, A. W., Yang, X., & Miles, N. J. (2016). The effect of bottom shape and baffle length on the flow field in stirred tanks in turbulent and transitional flow. *International Journal of Mechanical and Mechatronics Engineering*, 10(9), 1651-1660. https://doi.org/10.5281/zenodo.1126537

Doran, P. M. (1995). *Bioprocess Engineering Principles*. Academic Press.

el Mezaini, N. (2006). Effects of soil-structure interaction on the analysis of cylindrical tanks. *Practice periodical on Structural Design and Construction*, 11(1), 50-57. https://doi.org/10.1061/(ASCE)1084-0680(2006)11:1(50)

Guha, D., Ramachandran, P. A., Dudukovic, M. P., & Derksen, J. J. (2008). Evaluation of large Eddy simulation and Euler‐Euler CFD models for solids flow dynamics in a stirred tank reactor. *AIChE Journal*, 54(3), 766-778. https://doi.org/10.1002/aic.11417. http://www.bakker.org/dartmouth06/engs199/09-blend.pdf

Jakobsen, H. A. (2008). *Chemical reactor modeling. Multiphase Reactive Flows*. Springer International Publishing.

Khapre, A., & Munshi, B. (2014). Numerical comparison of Rushton turbine and CD-6 impeller in non-Newtonian fluid stirred tank. International Journal of *Chemical and Molecular Engineering*, 8(11), 1260-1267. https://doi.org/10.5281/zenodo.1097247

Landucci, G., Antonioni, G., Tugnoli, A., & Cozzani, V. (2012). Release of hazardous substances in flood events: Damage model for atmospheric storage tanks. *Reliability Engineering & System Safety*, 106, 200-216. https://doi.org/10.1016/j.ress.2012.05.010

Lane, G., & Koh, P. T. L. (1997, july*). CFD simulation of a Rushton turbine in a baffled tank*. Proceedings International Conference on Computational Fluid Dynamics in Mineral and Metal Processing and Power Generation, CSIRO, Melbourne, Australia. https://www.cfd.com.au/cfd_conf97/papers/lan035.pdf

Liangchao, L., Ning, C., Kefeng, X., & Beiping, X. (2019). CFD study on the flow field and power characteristics in a rushton turbine stirred tank in laminar regime. *International Journal of Chemical Reactor Engineering*, 17(11), 1-17. https://doi.org/10.1515/ijcre-2018-0215

Martínez-Nelis, F. M. (2010). *Estudio numérico de la fluidodinámica de un estanque de agitación utilizando método de mallas deslizantes* [Bachelor thesis, Universidad de Chile]. https://repositorio.uchile.cl/handle/2250/103931

McCabe, W. L., Smith, J. C., & Harriott, P. (2007). *Unit Operations of Chemical Engineering*. McGraw-Hill.

Mendoza-Escamilla, V. X., Alonzo-García, A., Mollinedo, H. R., González-Neria, I., Yáñez-Varela, J. A., & Martinez-Delgadillo, S. A. (2018). Assessment of k–ε models using tetrahedral grids to describe the turbulent flow field of a PBT impeller and validation

through the PIV technique. *Chinese Journal of Chemical Engineering*, 26(5), 942-956. https://doi.org/10.1016/j.cjche.2018.02.012

Micale, G., Montante, G., Grisafi, F., Brucato, A., & Godfrey, J. (2000). CFD simulation of particle distribution in stirred vessels. *Chemical Engineering Research and Design*, 78(3), 435-444. https://doi.org/10.1205/026387600527338

Montante, G., Lee, K. C., Brucato, A., & Yianneskis, M. (2001). Numerical simulations of the dependency of flow pattern on impeller clearance in stirred vessels. *Chemical Engineering Science*, 56(12), 3751-3770. https://doi.org/10.1016/S0009-2509(01)00089-6

Mustafa, S., Taha, M. M., Zatout, A. A., Sedahmed, G. H., & El-Gayar, D. A. (2021). Mass transfer at the outer surface of a spiral tube heat exchanger in a stirred tank reactor and possible applications. *Chemical Engineering Research and Design*, 165, 426-434. https://doi.org/10.1016/j.cherd.2020.11.023

Naeeni, S. K., & Pakzad, L. (2019). Droplet size distribution and mixing hydrodynamics in a liquid–liquid stirred tank by CFD modeling. *International Journal of Multiphase Flow*, 120, 103100. https://doi.org/10.1016/j.ijmultiphaseflow.2019.103100

Nagy, P., & Juhasz, J. (2016). Review of present knowledge on machine milking and intensive milk production in dromedary camels and future challenges. *Tropical Animal Health and Production*, 48(5), 915-926. https://doi.org/10.1007/s11250-016-1036-3

Nili-Ahmadabadi, M., Durali, M., & Hajilouy, A. (2014). A novel aerodynamic design method for centrifugal compressor impeller. *Journal of Applied Fluid Mechanics*, 7(2), 329-344. https://doi.org/10.36884/JAFM.7.02.20279

Paul, E. L., Atiemo-Obeng, V. A., & Kresta, S. M. (2004). *Handbook of Industrial Mixing: Science and Practice*. John Wiley & Sons.

Prabhu, M., Sreenath, K., Ajith Kumar, R., Jayakumar, J. S., & Joshy, P. J. (2021). Rankine vortex suppression in tanks with conical base: a numerical investigation. *Journal of Spacecraft and Rockets*, 58(2), 326-333. https://doi.org/10.2514/1.A34794

Pukkella, A. K., Vysyaraju, R., Tammishetti, V., Rai, B., & Subramanian, S. (2019). Improved mixing of solid suspensions in stirred tanks with interface baffles: CFD simulation and experimental validation. *Chemical Engineering Journal*, 358, 621-633. https://doi.org/10.1016/j.cej.2018.10.020

Qi, N., Zhang, H., Zhang, K., Xu, G., & Yang, Y. (2013). CFD simulation of particle suspension in a stirred tank. *Particuology*, 11(3), 317-326. https://doi.org/10.1016/j.partic.2012.03.003

Singh, H., Fletcher, D. F., & Nijdam, J. J. (2011). An assessment of different turbulence models for

predicting flow in a baffled tank stirred with a Rushton turbine. *Chemical Engineering Science*, 66(23), 5976-5988. https://doi.org/10.1016/j.ces.2011.08.018

Sivakumar, V., Visagavel, K., & Selvakumar, A. (2017). Analysis of Ventilation Rate in Cross Ventilated Rooms by Varying Aperture Shape of Windows using CFD. *Journal of Applied Fluid Mechanics*, 10, 61-68. https://doi.org/10.36884/JAFM.10.SI.28271

Su, T., Yang, F., Li, M., & Wu, K. (2018). Characterization on the hydrodynamics of a covering-plate Rushton impeller. *Chinese Journal of Chemical Engineering*, 26(6), 1392-1400. https://doi.org/10.1016/j.cjche.2017.11.015

Tahani, M., & Moradi, M. (2016). Aerodynamic investigation of a wind turbine using CFD and modified BEM methods. *Journal of Applied Fluid Mechanics*, 9(1), 107-111. https://doi.org/10.36884/jafm.9.SI1.25820

Todaro, C. M., & Vogel, H. C. (2014). *Fermentation and biochemical engineering handbook*. William Andrew.

Van den Akker, H. E. (2006). The details of turbulent mixing process and their simulation. *Advances in Chemical Engineering*, 31, 151-229. https://doi.org/10.1016/S0065-2377(06)31003-4

Venneker, B. C., Derksen, J. J., & Van den Akker, H. E. (2010). Turbulent flow of shear-thinning liquids in stirred tanks—The effects of Reynolds number and flow index. *Chemical Engineering Research and Design*, 88(7), 827-843. https://doi.org/10.1016/j.cherd.2010.01.002

Versteeg, H. K., & Malalasekera, W. (2007). *An introduction to computational fluid dynamics: the finite volume method*. Prentice Hall.

Wu, H., & Patterson, G. K. (1989). Laser-Doppler measurements of turbulent-flow parameters in a stirred mixer. *Chemical Engineering Science*, 44(10), 2207-2221. https://doi.org/10.1016/0009-2509(89)85155-3

Xia, B., & Sun, D. W. (2002). Applications of computational fluid dynamics (CFD) in the food industry: a review. *Computers and Electronics in Agriculture*, 34(1-3), 5-24. https://doi.org/10.1016/S0168-1699(01)00177-6

Youcef, K., Bouzit, M., Hadjeb, A., Arab, I. M., & Beloudane, M. (2016). CFD study of the effect of baffles on the energy consumption and the flow structure in a vessel stirred by a Rushton turbine. *Mechanics*, 22(3), 190-197. https://doi.org/10.5755/j01.mech.22.3.12663

Zadghaffari, R., Moghaddas, J. S., & Revstedt, J. (2009). A mixing study in a double-Rushton stirred tank. *Computers & Chemical Engineering*, 33(7), 1240-1246. https://doi.org/10.1016/j.compchemeng.2009.01.017